Journal of Materials Chemistry C

Accepted Manuscript

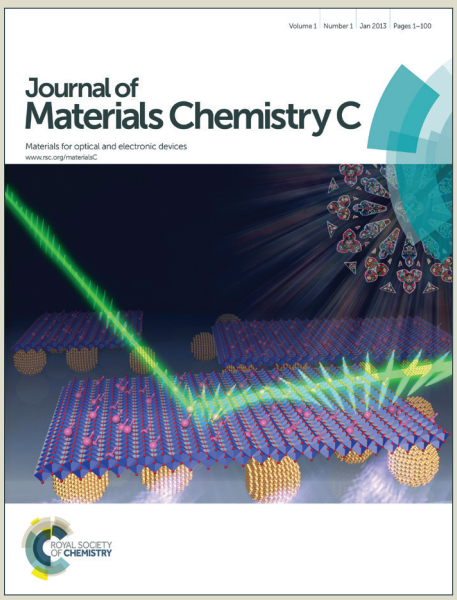

ROYAL SOCIETY OF CHEMISTRY

www.rsc.org/materialsC

Journal Name

RSCPublishing

COMMUNICATION

A low-temperature co-precipitation approach to synthesize fluoride phosphors $K_2MF_6:Mn^{4+}$ (M = Ge, Si) for white LED applications†

Cite this: DOI: 10.1039/x0xx00000x

Received 00th January 2012,
Accepted 00th January 2012

DOI: 10.1039/x0xx00000x

www.rsc.org/

Ling-Ling Wei,[a] Chun Che Lin,[b] Mu-Huai Fang,[b] Mikhail G. Brik,[c] Shu-Fen Hu,[d] Huan Jiao*[a] and Ru-Shi Liu*[be]

A new class of Mn^{4+} activated alkali-metal hexafluoride red phosphors are emerging for white light-emitting diodes because of their sharp red line $^2E_g \rightarrow {}^4A_{2g}$ emissions (600-650 nm) excited by irradiation of $^4A_{2g} \rightarrow {}^4T_{1g}$ (320-380 nm) and $^4A_{2g} \rightarrow {}^4T_{2g}$ (380-500 nm) transitions. However, these phosphors have the drawbacks of difficult control of the Mn valence state during synthesis and lack of underlying mechanisms for structure–photoluminescence relationships. In this study, we explore a novel, highly productive route to the quantifiable synthesis of $K_2GeF_6:Mn^{4+}$ by chemical co-precipitation method at room temperature. The prepared yellowish $K_2GeF_6:Mn^{4+}$ powders exhibit hexagonal shape and high crystalline without significant defects. The photoluminescence thermal stability and white light-emitting diodes applicability of $K_2GeF_6:Mn^{4+}$ suggest that it is a promising commercial red phosphor because of its efficient emission intensity, high color purity and excellent thermal stability. Structural analyses and theoretical calculations reveal that the red shift of $K_2GeF_6:Mn^{4+}$ red phosphor compared with $K_2SiF_6:Mn^{4+}$ is due to the longer Ge-F distance and lower effective Mulliken Charge of F ions in coordination environments of MnF_6^{2-} octahedron. The split feature in $K_2GeF_6:Mn^{4+}$ is due to the hexagonal distortion in the host. The structure-photoluminescence mechanism is predicted to be general in hexafluoride red phosphors to tune optical properties through cationic substitutions and crystal structure adjustments.

---

[a]*School of Chemistry and Chemical Engineering, Shaanxi Normal University, Xi'an 710062 Shaanxi, P.R. China*
E-mail: jiaohuan@snnu.edu.cn
[b]*Department of Chemistry, National Taiwan University, Taipei 106, Taiwan. E-mail: rsliu@ntu.edu.tw*
[c]*College of Mathematics and Physics, Chongqing University of Posts and Telecommunications, Chongqing 400065, P.R. China and Institute of Physics, University of Tartu, Ravila 14C, Tartu, 50411, Estonia*
[d]*Department of Physics, National Taiwan Normal University, Taipei 116, Taiwan*
[e]*Department of Mechanical Engineering and Graduate Institute of Manufacturing Technology, National Taipei University of Technology, Taipei 106, Taiwan*

†Electronic Supplementary Information (ESI) available: [details of any supplementary information available should be included here]. See DOI: 10.1039/c000000x/

1. Introduction

To fabricate warm white light-emitting diodes (WLEDs) with higher color-rendering index (CRI, $R_a > 80$), rare-earth activated nitride red phosphors, such as $MAlSiN_3:Eu^{2+}$ (M = Ca, Sr) and $M_2Si_5N_8:Eu^{2+}$ (M = Ca, Sr, Ba), are commercially added due to their sufficient chemical durability and efficient luminescent properties.[1-6] But these phosphors suffer from disadvantages given as follows: (1) demanding synthesis conditions isolated from air and moisture increase the production cost; (2) very broad emission spectrum (full width at half maximum ~80 nm) and a large part of the spectrum beyond 650 nm reduces the luminous efficiency of radiation. Hence, alternative red phosphors with high luminescence efficiency from 600 nm to 650 nm, good thermal stability and low production cost should be explored.

Mn^{4+} (electronic configuration, $3d^3$) exhibits sharp emission lines at 600-680 nm because of its distinctive electronic structure. In contrast to the inner $4f \rightarrow 4f$ forbidden transition of Eu^{3+}, the outer $3d \rightarrow 3d$ transition of Mn^{4+} is sensitive to local crystal field environments in the host and can be tuned by various substitutions.[7-12] Studies have focused on the preparation and optical properties of Mn^{4+} activated fluoride phosphors. Adachi et al. synthesized a series of Mn^{4+} activated red fluoride phosphors $A_2XF_6:Mn^{4+}$ (A = K, Na, Cs or NH_4; X = Si, Ge, Zr or Ti) and $BSiF_6:Mn^{4+}$ (B = Ba or Zn) by wet-chemical etching of silicon wafers. However, this method was inappropriate for quantifiable production because of the high cost of metal wafers and low luminescence efficiency caused by difficulty in controlling the valence state of Mn during synthesis.[13-17] The crystal structure of the host and the optical properties of Mn^{4+} emitters in fluoride phosphors remain unclear.[13-19] Hence, the structure-luminescence relationships should be analyzed to properly tune the optical properties of Mn^{4+} activated fluoride phosphors and meet the requirements of red phosphor. The characteristics and

drawbacks of $K_2GeF_6:Mn^{4+}$ and other red phosphors are compared differently in Table S1. It points on how $K_2GeF_6:Mn^{4+}$ overcomes the drawbacks that other red phosphors have.

In this study, we used the chemical co-precipitation method to synthesize $K_2GeF_6:Mn^{4+}$ with high purity and good crystalline without significant defects. The prepared yellowish $K_2GeF_6:Mn^{4+}$ powders exhibited an efficient emission intensity, high color purity and excellent thermal stability; these substances could be used in commercial applications. As the germanium oxide is easily dissolved in concentrated HF solution, the novel chemical co-precipitation method was operated at room temperature and suitable for quantifiable production because of its high yield, good repeatability and low cost. Particularly, in order to analyze the effects of the host crystal structure on the optical properties of Mn^{4+} emitters, crystal field and *ab* inito calculations combined with synchrotron X-ray diffraction (XRD) refinement and extended X-ray absorption fine structure (EXAFS) analysis were used to probe the optical features of $K_2GeF_6:Mn^{4+}$ and $K_2SiF_6:Mn^{4+}$.

The valence states of Mn (2+, 3+, 4+, 6+ and 7+) are sensitive to the synthesis temperature. Hence, the main difficulty lies in the controlling of Mn valence state for synthesizing Mn^{4+} activated fluoride compounds.[19] Thus two-step strategy of synthesizing K_2MnF_6 initially and then precipitating $K_2(Ge/Si)F_6:Mn^{4+}$ was proposed, and the synthesis temperature was not higher than 55 °C to avoid Mn^{4+} reduction. The specific operation route is shown in the Supporting Information. Figures S1 to S3 reveal that the synthesis temperature can tune the emission intensity of $K_2(Ge/Si)F_6:Mn^{4+}$ red phosphors by synchronously controlling the morphology and valence state of Mn. The optimal synthesis temperature for $K_2GeF_6:Mn^{4+}$ and $K_2SiF_6:Mn^{4+}$ red phosphors are 25 °C and 52 °C, respectively; these phosphors were used to investigate the structural and optical properties in this study. The two-step chemical co-precipitation strategy to synthesize $K_2GeF_6:Mn^{4+}$ red phosphor exhibits advantages given as follows: (1) the optimal synthesis temperature is room temperature, which can effectively reduce the volatilization of HF; (2) the amount of HF consumed to synthesize $K_2GeF_6:Mn^{4+}$ red phosphor is half of that used to synthesize $K_2SiF_6:Mn^{4+}$, which is safe and environmental-friendly; (3) $K_2GeF_6:Mn^{4+}$ red phosphor synthesized by two-step chemical co-precipitation method at room temperature exhibits efficient emission intensity and high thermal stability, which are beneficial to commercial applications.

2. Experimental

Two-step chemical co-precipitation method was used to synthesize $K_2(Ge/Si)F_6:Mn^{4+}$ red phosphors by initially synthesizing K_2MnF_6 and then precipitating $K_2(Ge/Si)F_6:Mn^{4+}$.

(1) Synthesis of K_2MnF_6: High-purity $KMnO_4$ and KHF_2 with mass ratio of 1:20 were dissolved in aqueous HF (48%) solution. The mixed solution was stirred and cooled for 0.5 h. The yellow powder K_2MnF_6 was precipitated by slowly dropping H_2O_2. After fast filtering and washing by acetone, the yellow powder was oven-dried for 2 h.

(2) Synthesis of $K_2(Ge/Si)_{0.95}F_6:Mn^{4+}{}_{0.05}$: GeO_2 (2.78 g) and KF (4.65 g) were dissolved in 15 mL HF (48%) aqueous solution at room temperature. After adding 0.2 g K_2MnF_6 powders in GeO_2/HF aqueous solution, the mixed solution was stirred at room temperature or in a water bath with fixed temperature between 0 °C and 60 °C. The KF/HF solution was added dropwise to the brown GeO_2/HF/K_2MnF_6 solution to precipitate yellow powder at the bottom of the container. Accordingly, the color of the mixture solution changed from brown to almost colorless. After pouring out the supernatant and washing thrice with ethanol, the yellow precipitate was oven-dried for 2 h. However, for the synthesis of $K_2Si_{0.95}F_6:Mn^{4+}{}_{0.05}$, 1.60 g SiO_2 was dissolved in 35 mL HF (48%) aqueous solution in a bath water at 70 °C. Other procedures were similar to the synthesis of $K_2Ge_{0.95}F_6:Mn^{4+}{}_{0.05}$.

(3) Structural and Optical Characterization. Synchrotron X-ray diffraction (XRD) patterns of the samples were collected with the Debye-Scherrer camera installed at the BL01C2 beamline of the National Synchrotron Radiation Research Center (NSRRC, Taiwan) with 0.774907 Å wavelength. The General Structure Analysis System software was used to analysis the X-ray Rietveld profile refinements of the structural modes. The extended x-ray absorption fine structure spectroscopy (EXAFS) results of Ge K-edge and Si K-edge were obtained at the BL01C and BL16A beamline stations of NSRRC, respectively. The morphologies of the samples were characterized by a scanning electron microscope (SEM, JSM-6700F). High-resolution transmission electron microscopy and selected area electron diffraction images were obtained via JEOL JEM-2011 microscope operated at 200 kV. The RT excitation and emission spectra were measured using a FluoroMax-3 spectrophotometer equipped with a 150 W Xe lamp. For temperature-dependent experiments at 80 K–300 K, the samples were placed in a small hold, the temperature of which was controlled by the liquid nitrogen cooling device. Light was radiated by Hamamatsu R928 photo-multiplier tube. The THMS-600 heating device was also used to study thermal quenching above 300 K.

3. Results and discussion

Figures 1a and 1b respectively show the X-ray Rietveld refinement results and the crystal structure of $K_2GeF_6:Mn^{4+}$. Figure S4 illustrates the related structure results of $K_2SiF_6:Mn^{4+}$. Yellowish $K_2GeF_6:Mn^{4+}$ powders yield bright red emission upon excitation of 460 nm light, indicating Mn^{4+} successfully doping into the crystal lattice of K_2GeF_6. The diffraction peaks of $K_2GeF_6:Mn^{4+}$ phosphor can be indexed to the hexagonal $P\bar{3}m1$ space group with lattice parameters of $a = b = 5.63171(6)$ Å, $c = 4.66751$ (6) Å, $\alpha = \beta = 90°$, $\gamma = 120°$ and $V = 128.2027$ (20) Å^3 (JCPDS NO. 73-1531). No traces of residual K_2MnF_6 and other impurities are observed. The crystal structure (Figure 1b) shows that each Ge^{4+} is surrounded by 6 F^- to form a regular GeF_6^{2-} octahedron. K^+ is at the center of 12 neighboring F^-. The prepared $K_2SiF_6:Mn^{4+}$ powders show lighter color than $K_2GeF_6:Mn^{4+}$, and emit bright red light under excitation of 460 nm light. The $K_2SiF_6:Mn^{4+}$ phosphor exhibits a high purity and belongs to cubic *F*m3m space group with lattice parameters of $a = b = c = 8.13107(7)$ Å, $\alpha = \beta = \gamma = 90°$ and $V = 537.579(8)$ Å^3 (JCPDS NO. 37-1155; Figure S4). Si^{4+} resides in the vertex and face-centered position of the cubic unit cell; and 4 K^+ ions are uniformly distributed inside the cube. Each Si^{4+} is surrounded by 6 F^- to form a regular SiF_6^{2-} octahedron. Furthermore, central Ge^{4+} and Si^{4+} possess different coordination environments as GeF_6^{2-} and SiF_6^{2-} octahedrons lie in various crystal structures. Measurements of the extended X-ray absorption fine structure (EXAFS) associated with Fourier-transform fitting were used to analyze the coordination environments of Ge^{4+} and Si^{4+}. Figure 1c suggests that the bond length between Ge^{4+} and ligand F^- ions (1.81 Å) is longer than that between Si^{4+} and F^- ions (1.66 Å). The differences between $K_2GeF_6:Mn^{4+}$ and $K_2SiF_6:Mn^{4+}$ phosphors in coordination environment and lattice symmetry of the host structure significantly influence their optical properties.

The Microstructures of $K_2GeF_6:Mn^{4+}$ were examined using scanning electron microscopy (SEM) and high resolution transmission electron microscope (HRTEM). SEM images indicate that the $K_2GeF_6:Mn^{4+}$ powders show hexagonal shape, and their

sizes range from 20 μm to 50 μm. By contrast, $K_2SiF_6:Mn^{4+}$ powders (Figure S4c) are of octahedral shape and the particle sizes are in the range of 10-30 μm. Typical HRTEM images reveal a very fine lattice arrangement of $K_2GeF_6:Mn^{4+}$, indicating a single crystal structure with highly crystalline and low structural defects. The selected area electron diffraction image (SAED; inset Figure 2b) exhibits specific shell-shaped-pattern spots corresponding to the [111] zone axis of the hexagonal $P\bar{3}m1$ space group. The crystal lattice spacing of (-220) plane is about 0.24 nm, which is consistent with the XRD results. Figure 2c shows the element mapping images of Ge, K, F and Mn for $K_2GeF_6:Mn^{4+}$. All elements show uniform distributions in the image contours, and the shapes of mapping images match well with the HRTEM images.

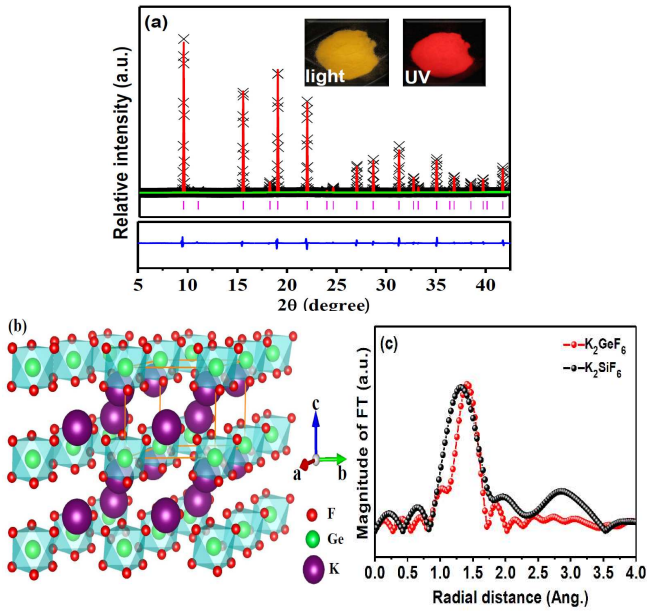

Fig. 1 Structure results of $K_2GeF_6:Mn^{4+}$ phosphor. (a) X-ray Rietveld refinements of $K_2GeF_6:Mn^{4+}$. (b) Structural schematic diagrams. (c) Fourier-transform-fitted EXAFS spectra for $K_2GeF_6:Mn^{4+}$ and $K_2SiF_6:Mn^{4+}$.

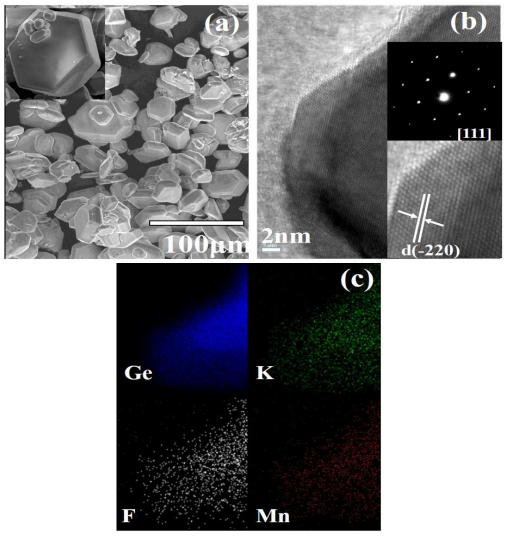

Fig. 2 (a) SEM images and (b) HRTEM images of $K_2GeF_6:Mn^{4+}$ phosphor; (inset) SAED pattern along [111] zone axis. (c) Element mapping images of Ge, K, F, and Mn for $K_2GeF_6:Mn^{4+}$.

Figure 3a illustrates the excitation and emission spectra of $K_2GeF_6:Mn^{4+}$ and $K_2SiF_6:Mn^{4+}$ red phosphors measured at room temperature. Consistent with the reported results of other Mn^{4+} activated fluoride compounds, there are two broad excitation bands located in the range of 320-500 nm, corresponding to the spin-allowed transitions of $^4A_{2g}\rightarrow{}^4T_{1g}$ and $^4A_{2g}\rightarrow{}^4T_{2g}$, respectively. The sharp red emission lines in the range of 600-650 nm are originated from the spin-forbidden $^2E_g\rightarrow{}^4A_{2g}$ transition. Different from the $^4A_{2g}\rightarrow{}^4T_{1g}$ transition spectra, the $^4A_{2g}\rightarrow{}^4T_{2g}$ transition of $K_2GeF_6:Mn^{4+}$ and $K_2SiF_6:Mn^{4+}$ red phosphors show several sharp occasionally peaks that are attributed to the asymmetric vibronic progression of the MnF_6 octahedron supposed on the electronic transition.[14] More importantly, the excitation and emission spectra of $K_2GeF_6:Mn^{4+}$ exhibit red shift compared to $K_2SiF_6:Mn^{4+}$.

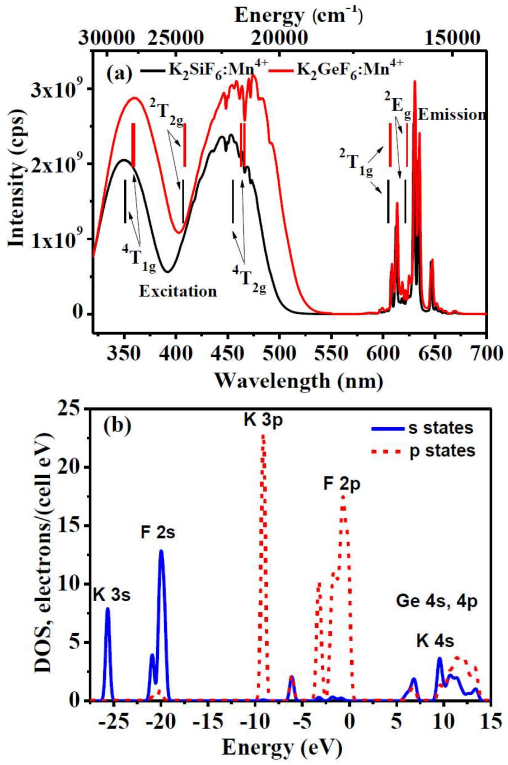

Fig. 3 (a) Experimental excitation and emission spectra of $K_2GeF_6:Mn^{4+}$ and $K_2SiF_6:Mn^{4+}$ phosphors (solid lines) compared with the calculated energy levels of Mn^{4+} (vertical bars). (b) Calculated partial DOS diagrams for K_2GeF_6.

To analyze the red shift behavior of $K_2GeF_6:Mn^{4+}$, crystal field calculations of the Mn^{4+} energy levels in K_2GeF_6 and K_2SiF_6 were obtained by diagonalizing the following crystal field Hamiltonian (Supporting Information).[20] The calculated energy levels (Table 1) reconfirm the red shift of $K_2GeF_6:Mn^{4+}$ phosphor. All the orbital triplets in K_2GeF_6 are split into singlets and doublets, as it should be in a hexagonal crystal field. While all orbital triplets are not split in cubic K_2SiF_6 since the octahedral symmetry is preserved at the Si position. The first explanation for red shift is that the Ge-F distance in K_2GeF_6 (1.81 Å) is longer than the Si-F distance in K_2SiF_6 (1.66 Å). Therefore, the crystal field effects in the former host are weaker, resulting in the red-shifted energy levels and excitation peaks in Table 1. *Ab* initio calculations have been indispensably used to assess the perspectives of materials' applications and limitations. We also used the CASTEP module of Materials Studio package.[21] Diagrams of the partial density of states (DOS; Figure 3b) allow to

identify the lowest electronic states in the K_2GeF_6 conduction band as those arising from the mixture of the K and Ge 4s states. The F 2p states, which are dominant in the valence band of both crystals, produce a minor contribution to the conduction band due to the hybridization effects. Very sharp (strongly localized) 3s and 3p electronic states of K and 2s states of F form narrow electronic bands at high energies. The effective Mulliken charges for all ions were calculated from the generalized gradient approximation (GGA) and local density approximation (LDA; Table S6). The absolute value of the effective fluorine charge in K_2GeF_6 is smaller than that in K_2SiF_6, which contributes to the weak crystal field in the former host and strong one in the latter host. Therefore, red shift of all $K_2GeF_6:Mn^{4+}$ spectral bands are consistently explained from the results of *ab* initio calculations.

Table 1. Calculated and experimental energy levels (in cm^{-1}) for Mn^{4+} in K_2GeF_6 and K_2SiF_6. The orbital doublet states are denoted with an asterisk. The Racah parameters are also given.

O_h group "parent"	K_2GeF_6 (B = 590; C = 3831)		K_2SiF_6 (B = 605; C = 3806)	
LS term	Calc.	Exp.	Calc.	Exp.
$^4A_{2g}$ (^4F)	0	0	0	0
^2E_g (^2G)	16050*	16050	16091	16091
$^2T_{1g}$(^2G)	16477*, 16489		16534	
$^4T_{2g}$(^4F)	21454*, 21598	~21505	21977	~21978
$^2T_{2g}$ (^2G)	24462, 24488*		24573	
$^4T_{1g}$ (^4F)	27808, 27922*	~27866	28475	~28490
$^4T_{1g}$(^4P)	45415*, 45723		46530	

Except for red shift, another interesting phenomenon is also found for $K_2GeF_6:Mn^{4+}$ red phosphor: broader excitation and emission bands compared with $K_2SiF_6:Mn^{4+}$. The peak positions are dependent on the coordination environments of MnF_6^{2-} octahedron, while the shape of emission spectra is associated with the crystal structure of the host. Mn^{4+} ions in K_2SiF_6 host with $Fm\bar{3}m$ space group have O_h symmetry, whereas the site symmetry of Mn^{4+} ions in K_2GeF_6 host with $P\bar{3}m1$ space group reduces to D_{3d}. The octahedral symmetry of O_h exhibits 6 fundamental internal vibronic modes $\nu_1(A_{1g})$, $\nu_2(E_g)$, $\nu_3(T_{1u})$, $\nu_4(T_{1u})$, $\nu_5(T_{2g})$ and $\nu_6(T_{2u})$. The ungerade vibrations of ν_3, ν_4 and ν_6 introduce some *u* character into the ^2E_g wave functions and then make the dipole allowed transition. In D_{3d} symmetry, the triply degenerate modes of ν_3, ν_4, ν_5 and ν_6 will split into doubly degenerate and non-degenerate modes as a result of small hexagonal distortion,[19] which results in stronger vibration transition coupling and broad emission lines.

To further reveal the electronic and vibronic structure of Mn^{4+} ions in different hosts, the temperature-dependent photoluminescence (PL) spectra were measured and shown in Figure S6. The integrated area of emission increase gradually between 80 K and 300 K in both $K_2GeF_6:Mn^{4+}$ and $K_2SiF_6:Mn^{4+}$ systems. The decreasing curve of $K_2GeF_6:Mn^{4+}$ is observed at temperature over 300 K. However, it is interesting that the decreasing curve of $K_2SiF_6:Mn^{4+}$ demonstrates at higher temperature over 470 K. Both of them have high thermal stability at LED operation temperature (150°C), and the intensity of emission is still over 90% of them at room temperature. Figures 4a and S7 respectively show the wavelength position and relative intensity of each emission line obtained at different temperatures for $K_2GeF_6:Mn^{4+}$ and $K_2SiF_6:Mn^{4+}$ red phosphors. The common feature is that all emission peaks show slight red shift and become broader with increasing temperature, which is reasonable as that the unit cell expands and the vibration modes enhance under heat treatment. $K_2GeF_6:Mn^{4+}$ exhibit unique split feature of peaks located at 610.0 nm, 610.3 nm, 635.0 nm and 647.0 nm, corresponding to the anti-strokes ν_4, ν_6 and strokes ν_4, ν_3 local vibronic emission peaks. The fundamental lattice modes of the transverse acoustic (TA) are more noticeable for Mn^{4+} in hexagonal K_2GeF_6 host with low crystal symmetry. The temperature-dependent behavior of integrated PL intensity I_{PL} (Figure 4b) shows considerable stability for $K_2GeF_6:Mn^{4+}$ red phosphor in the temperature range of 120-420 K. The relative I_{PL} at 420 K is above 96%, which is higher than that of rare-earth doped inorganic phosphors. As the vibronic emissions dominate the PL spectra of Mn^{4+} in fluorides, both the emission intensity and emission shape are responsible for the I_{PL} intensity. With increasing temperature from 80 K to 270 K, the anti-strokes emissions increase dramatically and all emission lines become broader as a result of the increased absorbed photons and enhanced vibration transition coupling associated with the vibration modes of MnF_6^{2-} octahedron, leading to the slight increase of I_{PL} intensity. Further increasing the temperature above 300 K will increase the non-radiative transition probability and the I_{PL} intensity shows thermal quenching, which can be fitted by $I_T/I_0 = [1 + D\exp(-E_a/kT)]^{-1}$, where I_0 is intensity at T = 0 K, *D* and activation energy E_a are refined variables. The activation energies obtained for $K_2GeF_6:Mn^{4+}$ red phosphor is 0.93 eV, which is 4 times higher than that of nitride compounds (~0.23 eV). Moreover, the external quantum efficiency of $K_2GeF_6:Mn^{4+}$ is 54% at room temperature. To evaluate the commercial application of the synthesized $K_2GeF_6:Mn^{4+}$ phosphor, the performances of WLEDs (fabricated with blue InGaN chips, $Y_3Al_5O_{12}:Ce^{3+}$ yellow phosphor and $K_2GeF_6:Mn^{4+}$ red phosphor) were examined. Electroluminescent spectra of the WLEDs reconfirm the sharp emission lines of Mn^{4+} in K_2GeF_6 phosphor. A bright "warm" white light with a CRI of 89 is obtained under a drive current of 15 mA (Figure 4c). The chromaticity coordinates of (0.4016, 0.4495) lies near the black body locus and the color temperature for WLEDs is 3974 K. Both the thermal stability and package results indicate the great promise of $K_2GeF_6:Mn^{4+}$ as commercial red phosphor in warm WLEDs.

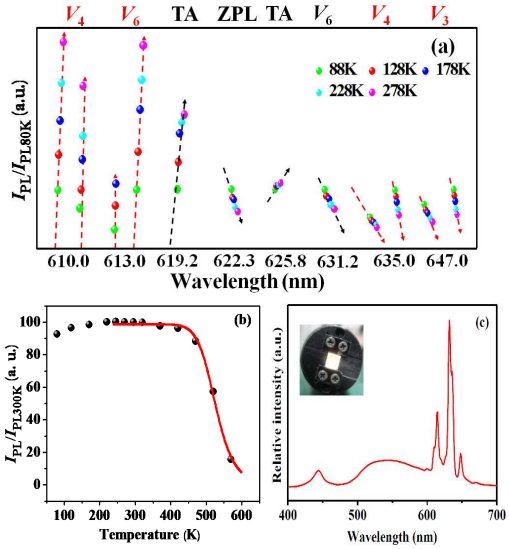

Fig. 4 (a) The wavelength position and relative intensity of each emission line obtained at different temperatures for $K_2GeF_6:Mn^{4+}$ red phosphor. (b) Temperature dependence of integrated PL intensity relative to room temperature for $K_2GeF_6:Mn^{4+}$. (c) Luminescence spectra of the White LEDs used $K_2GeF_6:Mn^{4+}$ red phosphor (inset: WLED image).

4. Conclusions

In summary, chemical co-precipitatfion method was used to synthesize $K_2GeF_6:Mn^{4+}$ red phosphor with high purity and good crystalline without significant defects. This method operated at room temperature was suitable for quantifiable production due to its high yield, good repeatability and low cost. The prepared yellowish $K_2GeF_6:Mn^{4+}$ powders had great promise as commercial red phosphor thanks to its efficient emission intensity, high color purity and excellent thermal stability. The structure analysis and theoretical calculations showed that the optical properties of Mn^{4+} activated fluoride phosphors were associated with the coordination environments of MnF_6^{2-} octahedron. The split feature in $K_2GeF_6:Mn^{4+}$ was caused by hexagonal distortion in the host. The structure-photoluminescence mechanism was predicted to be general in hexafluoride red phosphors to tune the optical properties through cation substitutions and crystal structure adjustments.

Acknowledgements

The authors would like to thank the National Science Council of the Ministry of Science and Technology of Taiwan (Contracts Nos. MOST 103-2112-M-003-009-MY3 and MOST 101-2113-M-002-014-MY3) for financially supporting this work. The financial support from the economic affairs of 101-EC-17-A-08-S1-183 is also appreciated. M. G. Brik appreciates support from the Marie Curie Initial Training Network LUMINET (grant agreement No. 316906), and the Programme for the Foreign Experts offered by Chongqing University of Posts and Telecommunications. We also thank Dr G. A. Kumar (University of Texas at San Antonio) for allowing using the Materials Studio package. Huan Jiao is grateful for financial support by the National Natural Science Foundation of China (Nos. 51272151) and the Fundamental Research Fund for the Central Universities (Nos. GK201402052, and GK201305013). Supported by the CAS/SAFEA International Partnership Program for Creative Research Teams is also appreciated.

References

1 J. Li, T. Watanabe, N. Sakamoto, H. Wada, T. Setoyama and M. Yoshimura, *Chem. Mater.* 2008, **20**, 2095-2105.
2 Y. Q. Li, N. Hirosaki, R. J. Xie, T. Takeda and M. Mitomo, *J. Solid State Chem.* 2009, **182**, 301-311.
3 M. Zeuner, P. J. Schmidt and W. Schnick, *Chem. Mater.* 2009, **21**, 2467-2473.
4 Z. J. Zhang, O. M. Ten Kate, A. C. A. Delsing, M. J. H. Stevens, J. T. Zhao, P. H. L. Notten, P. Dorenbos and H. T. Hintzen, *J. Mater. Chem.* 2012, **22**, 23871-23876.
5 N. Tapia-Ruiz, M. Segales and D. H. Gregory, *Coord. Chem. Rev.* 2013, **257**, 1978-2014.
6 S. S. Wang, W. T. Chen, Y. Li, J. Wang, H. S. Sheu and R. S. Liu, *J. Am. Chem. Soc.* 2013, **135**, 12504-12507.
7 Z. Bryknar, V. Trepakov, Z. Potucek and L. Jastrabik, *J. Lumin.* 2000, **87**, 605-607.
8 Y. Zhydachevskii, D. Galanciak, S. Kobyakov, M. Berkowski, A. Kaminska, A. Suchocki, Y. Zakharko and A. Durygin, *J. Phys.: Condens. Matter.* 2006, **18**, 11385-11396.
9 A. A. Setlur, E. V. Radkov, C. S. Henderson, J. H. Her, A. M. Srivastava, N. Karkada, M. S. Kishore, N. P. Kumar, D. Aesram, A. Deshpande, B. Kolodin, L. S. Grigorov and U. Happek, *Chem. Mater.* 2010, **22**, 4076-4082.
10 Y. Arai and S. Adachi, *J. Lumin.* 2011, **131**, 2652-2660.
11 M. G. Brik and A. M. Srivastava, *Opt. Mater.* 2013, **35**, 1251-1256.
12 M. H. Du, *J. Mater. Chem: C.* 2014, **2**, 2475-2481.
13 T. Takahashi and S. Adachi, *J. Electrochem. Soc.* 2008, **155**, E183-E188.
14 S. Adachi and T. Takahashi, *J. Appl. Phys.* 2009, **106**, 013516-1~6.
15 Y. K. Xu and S. Adachi, *J. Electrochem. Soc.* 2011, **158**, J58-J65.
16 R. Kasa and S. Adachi, *J. Electrochem. Soc.* 2012, **159**, J89-J95.
17 D. Sekiguchi, J. I. Nara and S. Adachi, *J. Appl. Phys.* 2013, **113**, 183516-1~6.
18 L. F. Lv, X. Y. Jiang, S. M. Huang, X. A. Chen and Y. X. Pan, *J. Mater. Chem: C.* 2014, **2**, 3879-3884.
19 H. M. Zhu, C. C. Lin, W. Q. Luo, S. T. Shu, Z. G. Liu, M. Wang, J. T. Kong, E. Ma, Y. G. Cao, R. S. Liu and X. Y. Chen, *Nat. Commun.* 2014, **5**, 4312-1~10.
20 B. Z. Malkin, A. A. Kaplyanskii and B. M. Macfarlane, *Spectroscopy of solids containing rare-earth ions,* Amsterdam: North-Holland, 1987; p. 13.
21 S. J. Clark, M. D. Segall, C. J. Pickard, P. J. Hasnip, M. J. Probert, K. Refson and M. C. Payne, *Z. Kristallogr. NCS.* 2005, **220**, 567-568.

TOC